UNIVERSITY OF MINNESOTA
ST. ANTHONY FALLS LABORATORY
Engineering, Environmental and Geophysical Fluid Dynamics

Project Report No. 550

Infiltration Rate Assessment for Woodland Cove

By

Lars Nielsen, Farzana Ahmed, Andrew J. Erickson and John S. Gulliver
St. Anthony Falls Laboratory
University of Minnesota
2 Third Avenue SE Minneapolis, MN 55455
http://www.safl.umn.edu/

Prepared for
James R. Hill Engineers

December 2010
Minneapolis, Minnesota

Table of Contents

Table of Contents III
Table of Figures III
Table of Tables IV
1 Introduction 1
2 Location 1
3 Methods 3
3.1 Strategy 4
3.2 Equipment 5
4 Analysis 7
4.1 Calculation of Saturated Hydraulic Conductivity values 7
4.2 Statistical Analysis 8
5 Results 12
6 References 16
7 Appendix A –Results for all the sites 17
8 Appendix B –Maps of the sites 33
9 Appendix C Soil distribution model 39
10 Appendix D Theoretical background 42

Table of Figures

Figure 2.1 Map showing sites of measurement 2
Figure 3.1 The Modified Philip-Dunne (MPD) Infiltrometer in place for *K* measurement. 3
Figure 3.2 Trench dug by the excavator 4
Figure 3.3 Installing the “new” MPD at the surface 5
Figure 3.4 MPD installed in hand-dug hole 6
Figure 4.1 Spreadsheet graph showing water level v. time 7
Figure 4.2 Histogram of all measurements of K 9
Figure 4.3 Log-transformation histogram of K data 9
Figure 5.1 Summary of Saturated Hydraulic Conductivity Measurements (mean values shown with 98% confidence intervals as errors bars) 13

Figure 5.2 Summary of Saturated Hydraulic Conductivity Measurements on a log scale (mean values shown with 98% confidence intervals as errors bars). 13
Figure 8.1 Map of site #1, #2 and #3 34
Figure 8.2 Map of site #4, #5 and #6. 35
Figure 8.3 Map of site #7, #9 and #10 36
Figure 8.4 Map of site #13, 1-3, 1-7 and 5-L-3 37
Figure 8.5 Map of site 3-18, 1-15 and 4-6. 38
Figure 9.1 3D-model of the distribution of soil types 40
Figure 9.2 3D model of the geology of the soil 41

Table of Tables

Table 4.1 Example of results from site #10 11
Table 5.1 Summary of results for all sites. 12
Table 5.2 Soil types as determined from the field test method (Thien 1970). Soil color is according to the Munsell chart Klute 1986), and soil depth is from the bottom of the top soil. 14
Table 7.1 Results and statistical analysis for site #1 17
Table 7.2 Results and statistical analysis for site #2 18
Table 7.3 Results and statistical analysis for site #3 19
Table 7.4 Results and statistical analysis for site #4 20
Table 7.5 Results and statistical analysis for site #5 21
Table 7.6 Results and statistical analysis for site #6 22
Table 7.7 Results and statistical analysis for site #7 23
Table 7.8 Results and statistical analysis for site #9 24
Table 7.9 Results and statistical analysis for site #10 25
Table 7.10 Results and statistical analysis for site 13 26
Table 7.11 Results and statistical analysis for site 1-3 27
Table 7.12 Results and statistical analysis for site 1-7 28
Table 7.13 Results and statistical analysis for site 1-15 29
Table 7.14 Results and statistical analysis for site 3-18 30
Table 7.15 Results and statistical analysis for site 4-6 31
Table 7.16 Results and statistical analysis for site 5-L-3 32

1 Introduction

Woodland Cove is a planned development along the western shore of Lake Minnetonka, within the city of Minnetrista. The pollutant loads of solids and total and dissolved phosphorous from the development entering the lake are to be kept to a minimum in order to meet the requirements from the local regulatory agencies, and therefore the developer is designing a series of infiltration practices for storm water runoff.

Within this project, a number of infiltration measurements were performed at several locations clustered at different sites in the area, to predict the efficiency of the planned practices. For this report, a 'location' is where an individual infiltration measurement was performed and a 'site' is a cluster of several infiltration measurements (locations). A high spatial variation in infiltration rate is normally observed, so a number of measurement locations were needed at each site to get a representative result. This report includes the results for the saturated hydraulic conductivity of the soil, *K*, measured at 16 different sites within the area. The results are presented in section 5.

2 Location

The area of consideration is located north of State Highway 7, and between Kings Point Road and Lotus Drive. The sites were chosen to represent the variety of the different soil types in the area, based on soil boring reports. A total of 73 soil borings were mapped, and a number of sites were proposed. Figure 9.1 and 9.2 in Appendix C shows the three dimensional maps of the soil borings used to identify representative locations.

The client also wanted to execute measurements where infiltration practices were planned, and added another set of sites which would require excavation to the depth of interest. Eventually, a total of 19 sites were planned, 6 of them located at the site of existing soil borings.

Figure 2.1 shows a map of various sites where the measurements were taken. The names of the points correspond to the results presented in section 5. On the map, sites #1 - #13 are located where infiltration practices were planned. The rest of the sites are located at the sites of existing soil borings.

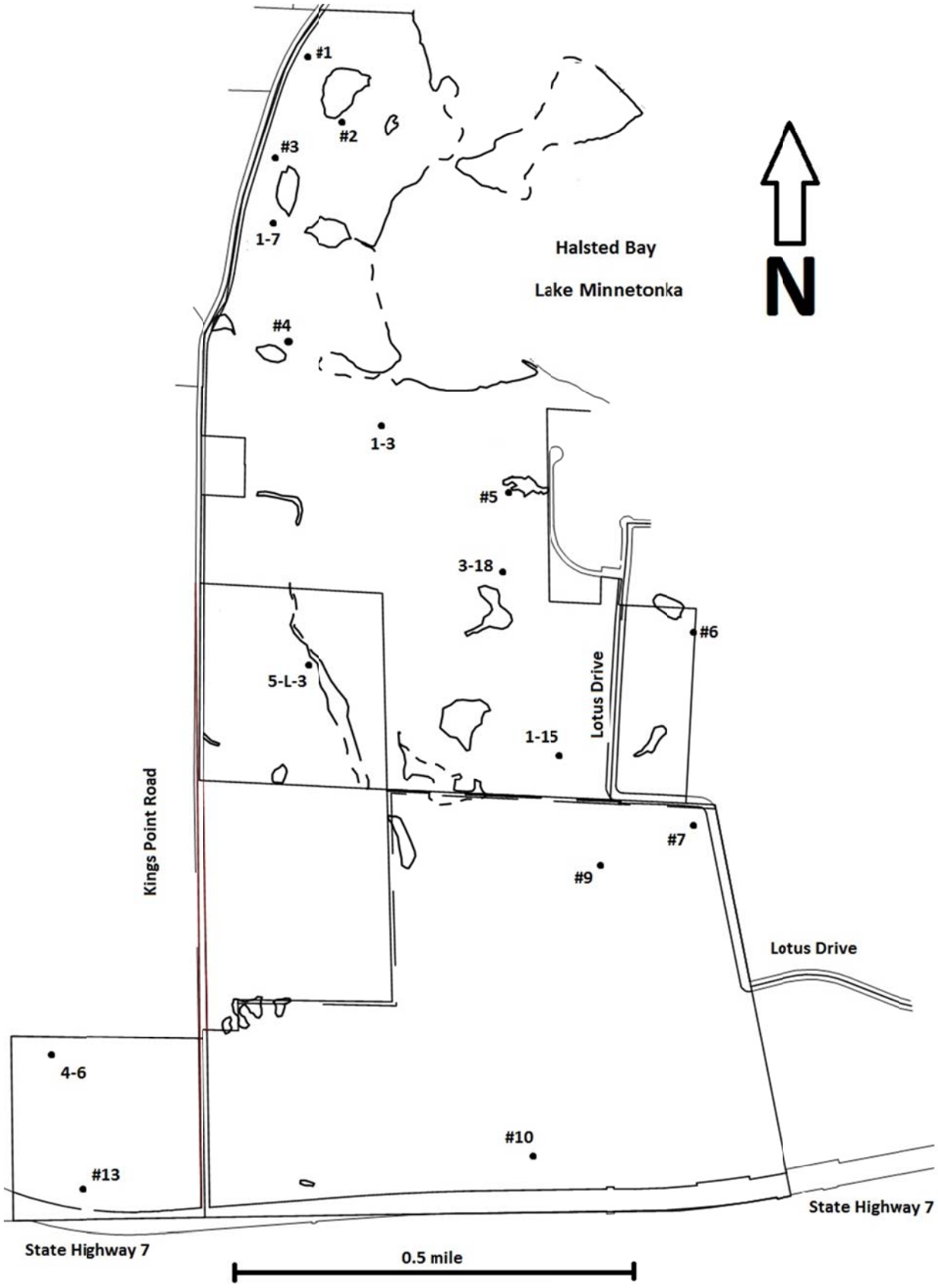

Figure 2.1 Map showing sites of measurement

3 Methods

The Modified Philip-Dunne Infiltrometer (MPD) was used for measuring the saturate hydraulic conductivity, *K*, of the soil. This is a falling head device that has to be filled with water followed by recording the height of water level in the device with respect to time. Using software developed by St. Anthony Falls Laboratory (Asleson, et al., 2009), the recordings of the water drop together with the initial and final moisture content in the soil were used to calculate values for *K*. The operation of the MPD is described in detail in a user's manual published by St. Anthony Falls Laboratory (Ahmed and Gulliver, 2010).

Figure 3.1 The Modified Philip-Dunne (MPD) Infiltrometer in place for *K* measurement.

3.1 Strategy

In this project, 16 different sites within the area were assessed. At each site, there were between six and twelve locations in which infiltration tests were performed to capture the high spatial variability of the infiltration rate. The sites were chosen based on the location of the proposed infiltrations practices, and a set of soil borings that had already been performed in the area.

Most of the planned infiltration practices were proposed at a lower elevation than the existing surface elevation, so that it was necessary to get through the topsoil to do the measurements in representative *in situ* soil. A grid of holes or trenches of about 5 feet was dug by an excavator, and the measurements were taken in the bottom of the holes. At some sites, the holes filled with groundwater, making measurements difficult or impossible with the current equipment. Because there is a great spatial variation in *K,* a goal of twelve measurements was set for each site. However, time constraints, difficult conditions, or experimental errors made the number of acceptable measurements smaller for many sites. The number of measurements of each site is included in the results in section 5.

Figure 3.2 Trench dug by the excavator

3.2 Equipment

Two different sets of MPD infiltrometers were used for these measurements. The “Old” MPDs are as described in Asleson, et al. (2009), and consisted of a single 40 cm long X 10 cm inside diameter cylinder made of aluminum. The “New” MPDs consisted of two parts: the top part is 37cm long constructed of clear PVC pipe and the detachable bottom is 7cm long made of finished steel. If the ground was dry and hard, the bottom part was first pounded into the ground and then the top part was placed into the bottom part using a rubber mallet, creating a sealed cylinder down into the soil. If the soil was wet, the rubber mallet was used with a block of wood to pound the entire MPD into the soil. A metric measuring tape is adhered to the outside of the clear acrylic pipe to allow measurement of the water level over time. A stop watch was available to place with each MPD infiltrometer to record the time and reduce measurement errors.

Figure 3.3 Installing the “new” MPD at the surface

The cylinder was filled with water, and the initial water level was noted down by the operator. Using the stopwatch with each infiltrometer, the water levels at a given time were recorded. Depending on the infiltration rate, the time interval between readings varied, but 12 to 15 readings were recorded to calculate a value for saturated hydraulic conductivity (*K).*

Both the initial and the final moisture content are needed to calculate the saturated hydraulic conductivity. Soil samples of around 80 to 130 grams were taken at each location before and after the measurements, and placed in small metal specimen containers. Analyses were performed to determine the volumetric moisture content (Klute 1986). As a part of these analyses, a bulk density value was obtained, following the procedure described by (ASTM, 2004). One bulk density sample was taken at each site, using a cylinder core sampler and a metal driver.

Figure 3.4 MPD installed in hand-dug hole

4 Analysis

4.1 Calculation of Saturated Hydraulic Conductivity values

The calculations of the *K* values were performed using a spreadsheet developed by Nestingen (2007) and revised by Ahmed and Gulliver (2010). It uses a Green-Ampt assumption of the development of the wetting front in the soil as water infiltrates, and computes a value for the saturated hydraulic conductivity based on the readings of water level vs. time, and values of initial and final moisture content.

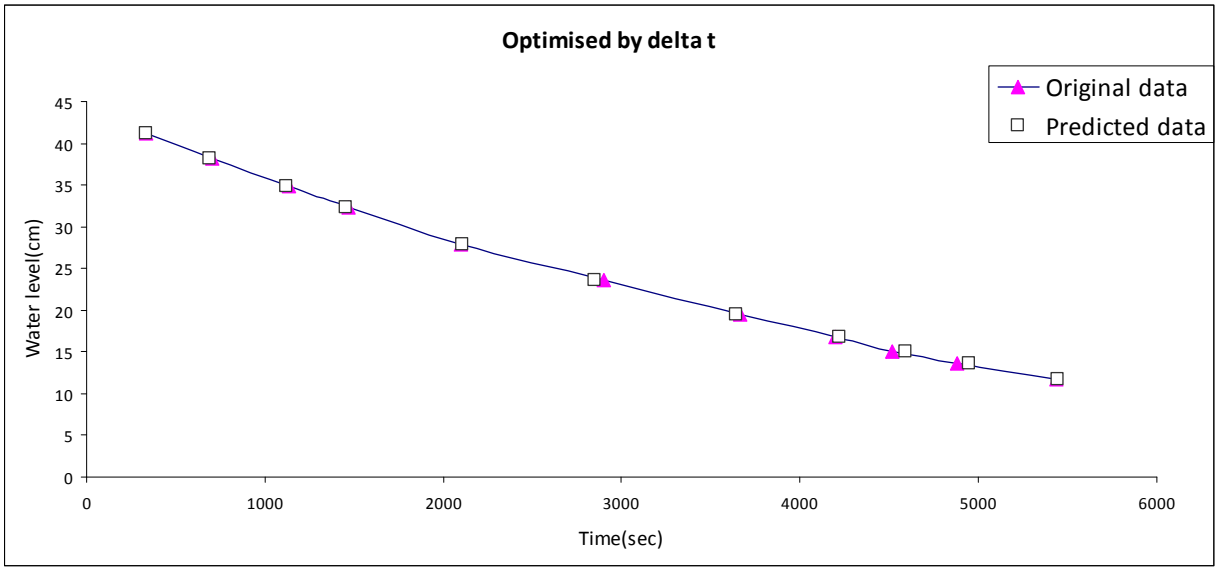

Figure 4.1 Spreadsheet graph showing water level v. time

Figure 4.1 provides a typical development of the water level versus time. The spreadsheet minimizes the root mean square (rms) of the difference between observed time increment (Δt) and predicted time increment as well as observed water level increment (ΔH) and predicted water level increment, by adjusting the saturated hydraulic conductivity (*K*) and soil suction (C). The theory behind the spreadsheet is described in more detail in Appendix C, and in the manual for the MPD (Ahmed and Gulliver, 2010).

In the field, at least 10 cm of water level drop was required for each measurement, to allow for an appropriate optimization of the *K* value with the spreadsheet. At locations where the water level dropped less than 10 cm in 6 hrs, the 1-dimensional Green-Ampt model was used to calculate *K* through the 5 cm of cylinder depth instead of using the spreadsheet.

4.2 Statistical Analysis

The appropriate mean to be used for the infiltration basins can be determined by an application of Darcy's law. Assume, for simplicity, that we have ten measurements representing equal areas of the projected basin. Then, the discharge through each area, Q_i, would be,

$$Q_i = -K_i A_i \frac{dh}{dz}\Big]_i \tag{1}$$

where *Q* = discharge, *K* = hydraulic conductivity, *A* = area and *dh/dz* is the vertical gradient of piezometric head. Now, assume that the gradient of piezometric head is constant everywhere, which means that the locations with a larger infiltration rate will infiltrate laterally into the locations with a smaller infiltration rate. Then, the total discharge of infiltration, *Q*, is,

$$Q = \sum_{i=1}^{N} Q_i = -A_i \frac{dh}{dz} \sum_{i=1}^{N} K_i \tag{2}$$

Because $A_i = A/N$,

$$Q = -\frac{A}{N}\frac{dh}{dz} \sum_{i=1}^{N} K_i = -A \frac{dh}{dz} \overline{K} \tag{3}$$

where $\overline{K}$ is the arithmetic mean of hydraulic conductivity.

The mean *K* for each site were thus calculated as arithmetic means, and all the measurements within one site were equally weighted, because the areas associated with each measurement did not have much effect on the arithmetic mean.

For identifying the *uncertainty* of these values, all the results of the *K* values are plotted in a histogram, showing the frequencies of occurrence in given intervals for the values of *K*. Figure 4.2 indicates that *K* follows a log-Normal distribution. To obtain a distribution that fits better to a normal distribution, a logarithmic transformation was preformed. By taking the $\log_{10}$(K) of all the values of *K*, the histogram in Figure 4.3 was plotted. Here, the frequencies of occurrence of given values of $\log_{10}$(K) are shown.

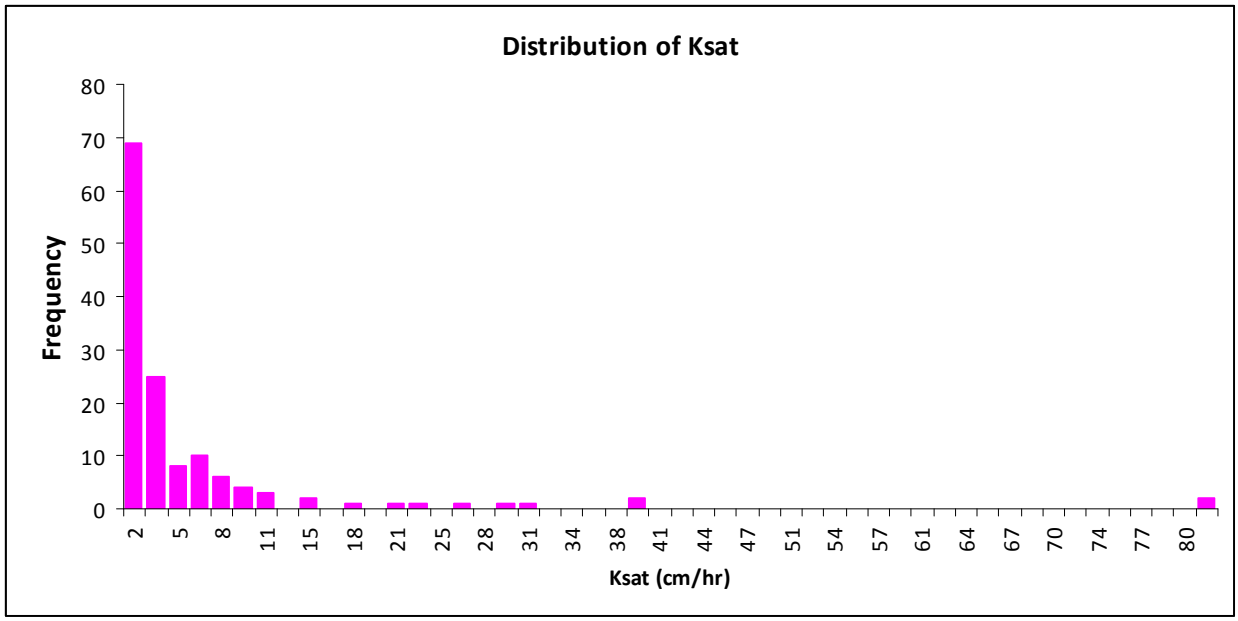

Figure 4.2 Histogram of all measurements of K

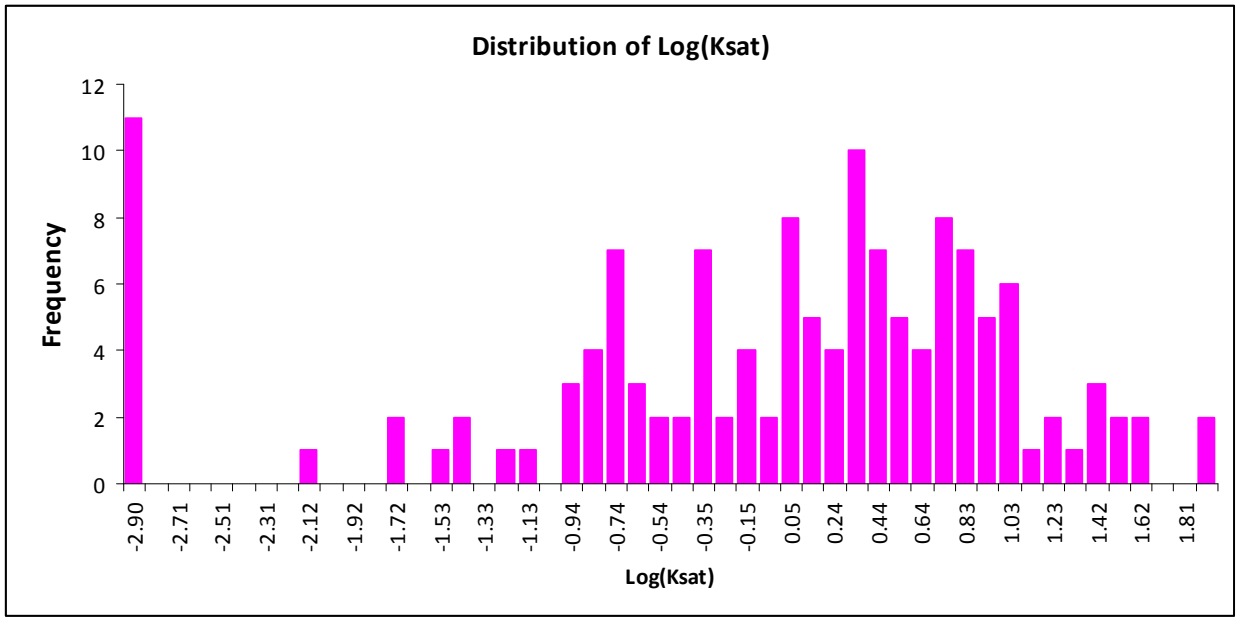

Figure 4.3 Log-transformation histogram of K data

Figure 4.3 indicates that the data is closer to a normal distribution in log space, and the statistical analyses were therefore preformed on this transformed distribution. The large number of values at -2.9 occurred because this was the lowest K value that could be measured, and it was assumed for all K values below this measurement.

Student's-t tests were then performed on the transformed data. This is a statistical hypothesis test that gives a range of uncertainty based on the variance in the dataset, the number of samples, and the given probability of exceedence. This resulted in upper and lower limits of confidence for the K values for each site, as presented in section 5.

For our transformed distribution, the Student's t test calculates the uncertainty of the mean value of a sample as:

$$C.I.\left(\log_{10}(K)\right) = \overline{\log_{10}(K)} \pm \frac{\sigma_{log} t}{\sqrt{N}} \quad (4)$$

where

$\overline{Log_{10}(K)}$ = the arithmetic mean of the Log_{10}(K) values in the sample

σ_{log} = the standard deviation of the logarithmic transformation

N = the number of measurements in the sample

t = Student's t value, determined by the number of samples and the given probability of exceedence (alpha)

C.I. = Confidence interval

The confidence interval was set to 98% (one out of fifty chance that the actual mean *K* will be outside the confidence interval), and the Student's t values were obtained from tables (Moore, McCabe and Craig, 2009).

For each site, the variance of the logarithmic values was calculated, and the confidence interval within the logarithmic distribution was obtained. Finally, the results were converted back to the original distribution, giving the range of *K* as presented in section 5.

Example of calculation of uncertainty

The results from site #10 are shown as an example. The calculations used the Student's t test on the transformed distribution.

Table 4.1 Example of results from site #10

Location	Saturated Hydraulic Conductivity(cm/hr), *K*	$Log_{10}(K)$
1	0.360	-0.444
2	3.620	0.559
3	2.030	0.307
4	0.001	-3.000
5	2.040	0.310
6	0.060	-1.222
7	7.690	0.886
9	1.070	0.029
10	1.100	0.041
11	1.110	0.045
12	0.150	-0.825

Here, 11 values of *K* were calculated, so N=11. The standard deviation of the distribution of $\log_{10}(K)$ were calculated from the column to the right, giving σ_{log}=1.08. The mean value of $\log_{10}(K)$ is -0.301, and the Student's t value for N=11 and a 98% confidence interval is 2.764.

The uncertainty was then calculated in the following manner.

$$C.I.\left(\ log_{10}(K_{sat})\right) = \overline{log_{10}(K_{sat})}\ \pm \frac{\sigma_{log} t}{\sqrt{n}}$$

$$C.I.\left(log_{10}(K_{sat})\right) = \frac{1}{11}\sum(log_{10}(K_{sat})) \pm \frac{1.08 * 2.764}{\sqrt{11}}$$

$$C.I.\left(log_{10}(K_{sat})\right) = -0.301 \pm 0.90$$

$$C.I.\left(K_{sat}\right) = 10^{-0.301 \pm 0.90}$$

$$Upper\ Limit\ (K_{sat}) = 3.971$$
$$Lower\ Limit\ (K_{sat}) = 0.063$$

5 Results

The final results for each site are presented in this Table 5.1. The expected mean value is calculated as an arithmetic mean. The rationale is given in Section 4. The confidence intervals were computed based upon a log-normal distribution of the measurements, as described in section 4, found to be more representative of the distribution than a normal distribution. The saturated hydraulic conductivities from Table 5.1 are plotted in Figures 5.1 and 5.2. Figure 5.2 is in a log scale so that the lower confidence interval can be visualized.

Figure 2.2 in section 2 show where each site is located. The results for every measurement within each site are included in Appendix A. Maps describing the distribution of measurements within each site are included in Appendix B.

Table 5.1 Summary of results for all sites.

Site number	**Number of Measurements**	**Mean K [cm/hr]**	**Upper Limit (cm/hr)** (98% confidence interval)	**Lower Limit (cm/hr)** (98% confidence interval)
#1	7	1.594	2.690	0.001
#2	10	1.472	3.898	0.005
#3	8	2.009	4.325	0.028
#4	9	2.973	6.047	0.086
#5	10	2.734	6.822	0.050
#6	6	2.683	45.329	0.003
#7	8	2.005	8.218	0.022
#9	8	7.466	18.242	0.487
#10	11	1.743	3.888	0.059
#13	8	2.033	4.500	0.239
1-3	8	7.856	21.038	0.294
1-7	11	3.436	7.147	0.545
1-15	12	3.015	4.488	0.265
3-18	6	1.963	8.182	0.110
4-6	8	37.07	63.720	13.125
5-L-3	8	4.180	6.639	0.001

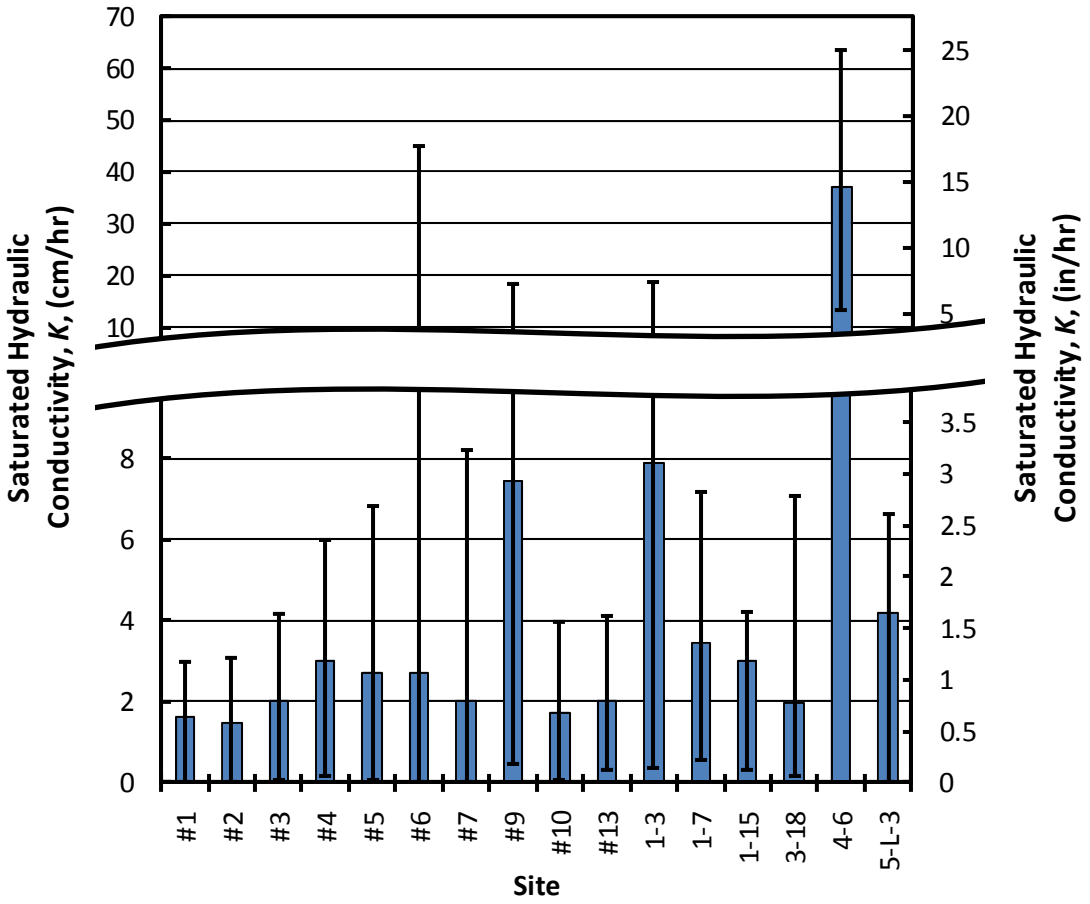

Figure 5.1 Summary of Saturated Hydraulic Conductivity Measurements (mean values shown with 98% confidence intervals as errors bars).

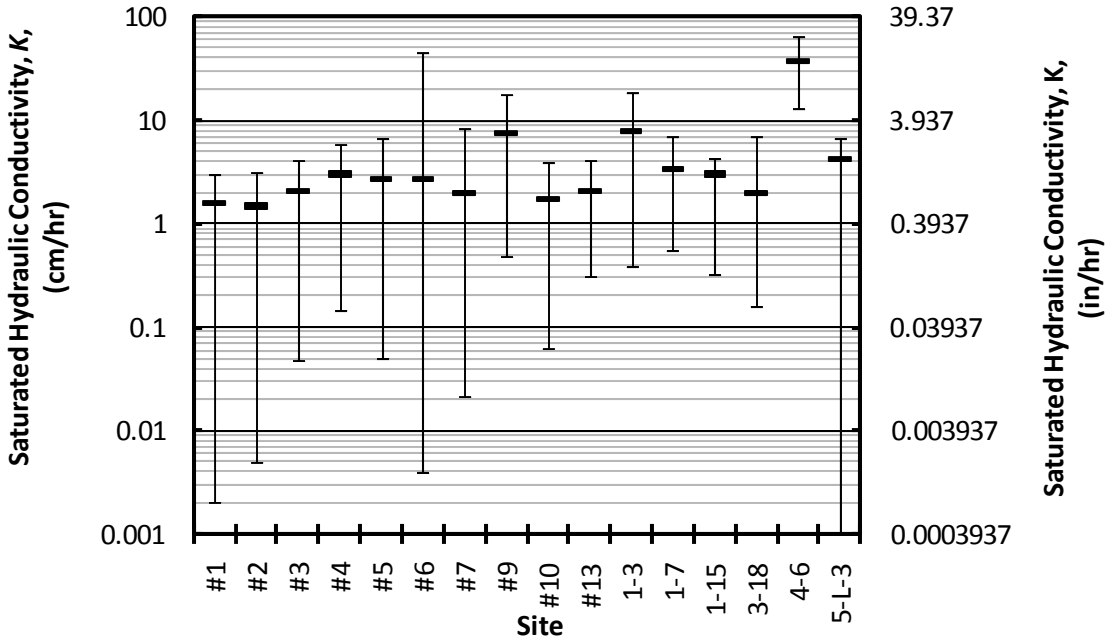

Figure 5.2 Summary of Saturated Hydraulic Conductivity Measurements on a log scale (mean values shown with 98% confidence intervals as errors bars).

Soil cores of the upper soil layers were taken for most of the sites. These cores were analyzed for soil color from the Munsell charts (Klute 1986) and soil type by the field test method (Thien 1970). The results, given in Table 5.2, indicate that most of the soils are classified as clays or clay loams. It is not surprising, then, that the lower confidence level for saturated hydraulic conductivity is small. The high mean saturated hydraulic conductivity is likely caused by soil structure, which is determined by how individual soil granules clump or bind together and aggregate, affecting, the arrangement of soil pores between them. Both soil texture and structure have a major influence on water and air movement, biological activity, and root growth.

Table 5.2 Soil types as determined from the field test method (Thien 1970). Soil color is according to the Munsell chart Klute 1986), and soil depth is from the bottom of the top soil.

Site	Depth	Soil color	Soil type
2	0 to 27 inch	Black	Sandy clay loam
	27 to 31 inch	Black	Sandy clay loam
	31 to 38 inch	Black	Sandy clay loam
3	0 to 26 inch	Olive brown	Silty clay
	26 to 46 inch	Light olive brown	Sandy clay loam
	46 to 51 inch	Light olive brown	Silt
	51 to 60 inch	Light olive brown	Silty clay loam
6	0 to 32 inch	Olive brown	Clay
	32 to 44 inch	Light olive brown	Silty clay loam
	44 to 55 inch	Olive brown	Silty clay loam/ Sandy clay loam
7	0 to 32 inch	Olive brown	Clay/ Silty clay
	32 to 60 inch	Light olive brown	Clay/ Silty clay
9	0 to 24 inch	Dark grayish brown	Clay
	24 to 40 inch	Light olive brown	Sandy clay loam
	40 to 50 inch	Light olive brown	Sandy clay loam
10	0 to 16 inch	Olive brown	Sandy clay loam
	16 to 24 inch	Olive brown	Clay/ Silty clay
	24 to 32 inch	Olive brown	Sandy clay loam
	32 to 46 inch	Light olive brown	Clay/ Silty clay
	46 to 50 inch	Light olive brown	Sandy clay loam
1-3	0 to 28 inch	Black	Silty clay loam/ Clay loam
	28 to 43 inch	Black	Clay
1-15	0 to 19 inch	Olive brown	Clay/Silty Clay
	19 to 22 inch	Olive brown	Clay/Silty Clay
	22 to 27 inch	Olive brown	Clay/Silty Clay
	27 to 32 inch	Olive brown	Clay/Silty Clay
3-18	0 to 7 inch	Very dark grayish brown	Clay
	7 to 12 inch	Very dark grayish brown	Clay
5-L-3	0 to 16 inch	Dark grayish brown	Clay
	16 to 24 inch	Very dark gray	Clay

Even though the underlying soil is predominantly clays, it is possible that the soil structure will allow the required 1.5 ft of infiltration for the design storm. The soil structure, however, will likely be broken down with compaction from heavy construction equipment. It is important that the construction personnel are aware of the importance of this fact for the proper operation of the infiltration basins.

Conclusion

The mean saturated hydraulic conductivities for each of the sites indicates that the soil under many of the sites is suitable for the shallow infiltration basins of the Woodland Cove development in the City of Minnetristra. The confidence intervals, however, are typically large because only one or two locations at many of the sites had a substantially larger saturated hydraulic conductivity than the others. This is an indication that the soil structure is non-uniform, and that infiltration will be through certain pathways, with the remainder of the soil lightly participating in infiltrating the water from a storm. The chances that one or two measurements may not represent the basin, or would not be located in the basin's location, are shown to be significant.

It is recommended that both the mean saturated hydraulic conductivity and the confidence interval be used to determine if a given location is suitable for an infiltration basin. It may be possible to construct infiltration facilities at locations 1, 2, 3, 4, 5, 6, 7, 10, 3-18 and 5-L-3 with under-drains under the engineered soil and a closure valve. The engineered soil can be chosen to filter particles and to remove dissolved phosphorus, resulting in relatively nutrient-free water directed to the receiving water body. Then, if infiltration does not occur sufficiently, the valve can be opened and the under-drains will pull water out after it is filtered and has trapped dissolved phosphorus through the engineered soil. This is one possibility to deal with the risk of poorly infiltrating soils in these infiltration basins.

6 References

Ahmed, Farzana and J.S. Gulliver. 2010. Manual for the Modified Philip-Dunne (MPD) Infiltrometer. St. Anthony Falls Laboratory (http://www.safl.umn.edu).

American Engineering Testing Inc, 2005. "Report of Geotechnical Exploration and Review". AET Job No. 20-05369.

American Engineering Testing Inc, 2002. "Report of Geotechnical Exploration and Review". AET Job No. 20-02770.

Asleson, B.C., R.S. Nestingen, J.S. Gulliver, R.M. Hozalski, and J.L. Nieber, "Assessment of Rain Gardens by Visual Inspection and Controlled Testing," *Journal of the American Water Resources Association,* 45(4), 1019-1031, 2009.

A.S.T.M. D 2937-04, 2004. Standard Test Method for Density of Soil in Place by the Drive-Cylinder Method. ASTM International Ed.

Braun Intertec. Engineering, Inc, 1993. "A preliminary Geotechnical Evaluation Report for Carlson Real Estate Company". Project BABX-93-563

Braun Intertec Corporation, 2000. "A preliminary Geotechnical Evaluation Report for Lundgren Brothers Construction, Inc". Project BABX-99-751A.

Braun Intertec. Corporation, 2006. "A Geotecnical Evaluation Report". Project BL-06-03051

Klute, A. 1986. Methods of Soil Analysis, Part I. Physical and Mineralogical Methods, 2.nd edition. Soil Science Society of America, Inc. Publisher, Madison, WI

Moore, McCabe, Craig. Introduction to the Practice of Statistics. Sixth edition. New York: W.H. Freeman and Company, 2009

Rebecca S. Nestingen, "The Comparison of Infiltration Devices and Modification of the Philip-Dunne Permeameter for the Assessment of Rain Gardens," M.S. Thesis, University of Minnesota, November 2007.

Thien, S. J. 1979. A flow diagram for teaching texture-by-feel analysis. J. Agron. Educ. 8:54-55.

7 Appendix A –Results for all the sites

Site #1

Table 7.1 Results and statistical analysis for site #1

Location	Saturated Hydraulic Conductivity(cm/hr)
A1	0.080
B1	0.008
B2	0.077
B3	9.940
C1	1.050
C2	0.001
C3	0.003

Statistical analysis of Saturated Hydraulic Conductivity (cm/hr)	
Arithmetic mean	**1.594**
Number of locations	7
Variance	13.688
Standard deviation	3.700
Student t	3.143
upper limit	3.690
lower limit	0.001

Site #2

Table 7.2 Results and statistical analysis for site #2

Location	Saturated Hydraulic Conductivity(cm/hr)
A1	3.110
A2	5.300
B1	0.001
B2	0.001
B3	1.020
B4	0.067
C1	4.420
C2	0.580
C3	0.220
C4	0.001

Statistical analysis of Saturated Hydraulic Conductivity (cm/hr)	
Arithmetic mean	1.472
Number of locations	10
Variance	4.118
Standard deviation	2.029
Student t	2.821
upper limit	2.898
lower limit	0.005

Site #3

Table 7.3 Results and statistical analysis for site #3

Location	Saturated Hydraulic Conductivity(cm/hr)
A1	0.101
A3	0.310
B1	7.990
B2	0.110
B3	0.008
C1	2.060
C2	5.400
C3	0.091

Statistical analysis of Saturated Hydraulic Conductivity (cm/hr)	
Arithmetic mean	2.009
Number of locations	8
Variance	9.298
Standard deviation	3.049
Student t	2.998
upper limit	4.325
lower limit	0.028

Site #4

Table 7.4 Results and statistical analysis for site #4

Location	Saturated Hydraulic Conductivity(cm/hr)
1	0.252
2	0.094
3	1.950
4	6.100
5	3.050
6	0.285
7	0.013
8	13.800
9	1.210

Statistical analysis of Saturated Hydraulic Conductivity (cm/hr)	
Arithmetic mean	2.973
Number of locations	9
Variance	20.356
Standard deviation	4.512
Student t	2.896
upper limit	6.047
lower limit	0.086

Site #5

Table 7.5 Results and statistical analysis for site #5

Location	Saturated Hydraulic Conductivity(cm/hr)
1	0.100
2	0.410
3	0.000
4	6.010
5	10.310
6	4.940
7	0.400
8	3.130
9	1.870
10	0.170

Statistical analysis of Saturated Hydraulic Conductivity (cm/hr)	
Arithmetic mean	2.734
Number of locations	10
Variance	11.748
Standard deviation	3.428
Student t	2.821
upper limit	6.822
lower limit	0.051

Site #6

Table 7.6 Results and statistical analysis for site #6

Location	Saturated Hydraulic Conductivity(cm/hr)
1	8.050
2	2.380
3	0.026
4	0.001
5	4.780
6	0.860

Statistical analysis of Saturated Hydraulic Conductivity (cm/hr)	
Arithmetic mean	2.683
Number of locations	6
Variance	10.174
Standard deviation	3.189
Student t	3.365
upper limit	45.329
lower limit	0.003

Site #7

Table 7.7 Results and statistical analysis for site #7

Location	Saturated Hydraulic Conductivity(cm/hr)
A1	9.250
B1	3.150
A2	1.320
B2	0.640
A3	0.130
B3	0.280
A4	1.270
B4	0.000

Statistical analysis of Saturated Hydraulic Conductivity (cm/hr)	
Arithmetic mean	2.005
Number of locations	8
Variance	9.598
Standard deviation	3.098
Student t	2.998
upper limit	8.218
lower limit	0.022

Site #9

Table 7.8 Results and statistical analysis for site #9

Location	Saturated Hydraulic Conductivity(cm/hr)
A2	0.350
A5	28.960
A6	9.600
B2	1.730
B3	9.090
B4	7.030
B5	0.210
B6	2.760

Statistical analysis of Saturated Hydraulic Conductivity (cm/hr)	
Arithmetic mean	7.466
Number of locations	8
Variance	89.673
Standard deviation	9.470
Student t	2.998
upper limit	18.241
lower limit	0.487

Site #10

Table 7.9 Results and statistical analysis for site #10

Location	Saturated Hydraulic Conductivity(cm/hr)
1	0.360
2	3.620
3	2.030
4	0.001
5	2.040
6	0.060
7	7.690
9	1.070
10	1.100
11	1.110
12	0.091

Statistical analysis of Saturated Hydraulic Conductivity (cm/hr)	
Arithmetic mean	1.743
Number of locations	11
Variance	5.083
Standard deviation	2.255
Student t	2.764
upper limit	3.888
lower limit	0.059

Site #13

Table 7.10 Results and statistical analysis for site 13

Location	Saturated Hydraulic Conductivity(cm/hr)
2	0.520
3	0.830
4	4.410
5	0.082
6	2.280
7	0.600
8	0.950
9	6.590

Statistical analysis of Saturated Hydraulic Conductivity (cm/hr)	
Arithmetic mean	2.033
Number of locations	8
Variance	5.321
Standard deviation	2.307
Student t	2.998
upper limit	4.500
lower limit	0.239

Site 1-3

Table 7.11 Results and statistical analysis for site 1-3

Location	Saturated Hydraulic Conductivity(cm/hr)
1	7.190
2	3.740
3	4.910
4	3.530
5	0.440
6	0.047
7	39.110
8	3.880

Statistical analysis of Saturated Hydraulic Conductivity (cm/hr)	
Arithmetic mean	7.856
Number of locations	8
Variance	164.768
Standard deviation	12.836
Student t	2.998
upper limit	21.038
lower limit	0.294

Site 1-7

Table 7.12 Results and statistical analysis for site 1-7

Location	Saturated Hydraulic Conductivity(cm/hr)
A1	2.250
A2	1.410
A3	2.220
A4	0.030
B1	9.760
B3	1.110
B4	1.990
C1	5.800
C2	5.210
C3	2.220
C4	5.800

Statistical analysis of Saturated Hydraulic Conductivity (cm/hr)	
Arithmetic mean	3.436
Number of locations	11
Variance	8.189
Standard deviation	2.862
Student t	2.764
upper limit	7.147
lower limit	0.545

Site 1-15

Table 7.13 Results and statistical analysis for site 1-15

Location	Saturated Hydraulic Conductivity(cm/hr)
A1	0.430
A2	0.180
A3	0.620
A4	5.990
B1	1.040
B2	2.100
B3	2.360
B4	1.680
C1	17.420
C2	1.680
C3	0.015
C4	2.660

Statistical analysis of Saturated Hydraulic Conductivity (cm/hr)	
Arithmetic mean	3.015
Number of locations	12
Variance	23.152
Standard deviation	4.812
Student t	2.718
upper limit	4.488
lower limit	0.265

Site 3-18

Table 7.14 Results and statistical analysis for site 3-18

Location	Saturated Hydraulic Conductivity(cm/hr)
A	1.960
B	0.250
C	5.960
D	1.360
E	2.160
F	0.085

Statistical analysis of Saturated Hydraulic Conductivity (cm/hr)	
Arithmetic mean	1.963
Number of locations	6
Variance	4.568
Standard deviation	2.137
Student t	3.365
upper limit	8.182
lower limit	0.110

Site 4-6

Table 7.15 Results and statistical analysis for site 4-6

Location	Saturated Hydraulic Conductivity(cm/hr)
A1	81.860
A2	22.860
A3	81.160
A4	26.030
B1	38.790
B2	21.250
B3	13.490
B4	11.130

Statistical analysis of Saturated Hydraulic Conductivity (cm/hr)	
Arithmetic mean	37.071
Number of locations	8
Variance	822.287
Standard deviation	28.676
Student t	2.998
upper limit	63.720
lower limit	13.125

Site 5-L-3

Table 7.16 Results and statistical analysis for site 5-L-3

Location	Saturated Hydraulic Conductivity(cm/hr)
A1	0.130
A2	1.380
A3	0.000
A4	1.880
B1	0.510
B2	29.540
B3	0.000
B4	0.000

Statistical analysis of Saturated Hydraulic Conductivity (cm/hr)	
Arithmetic mean	4.180
Number of locations	8
Variance	105.507
Standard deviation	10.272
Student t	2.998
upper limit	6.639
lower limit	0.001

8 Appendix B –Maps of the sites

This section describes the distribution of measurements within each site. Refer to appendix A to see the measured values of K for each location.

Time constrains and holes that were filled with water made it difficult to do as many measurements in each site as would have been optimal. For each site, the maps are showing which of the holes that are represented in the results.

In the maps, circles with a cross represent holes were measurements were taken. Site #11, #12 and #8 are not included in the maps, as all the holes were filled full with water.

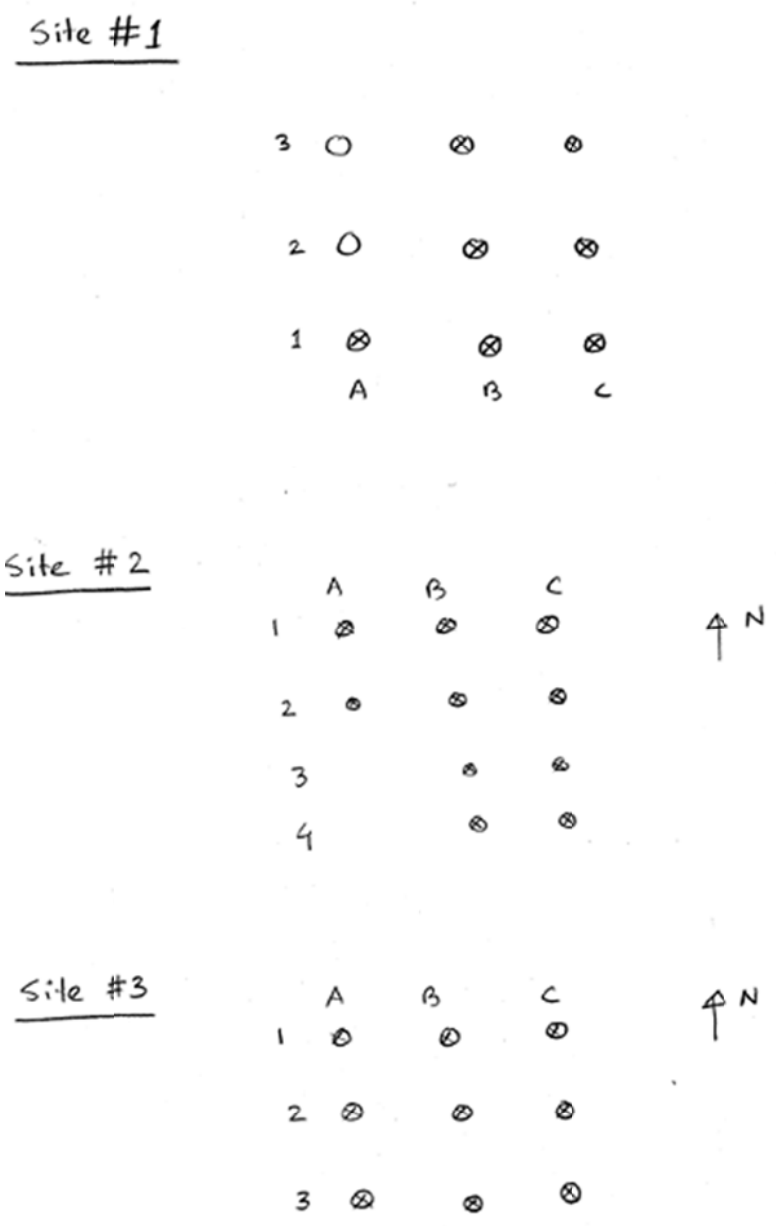

Figure 8.1 Map of site #1, #2 and #3

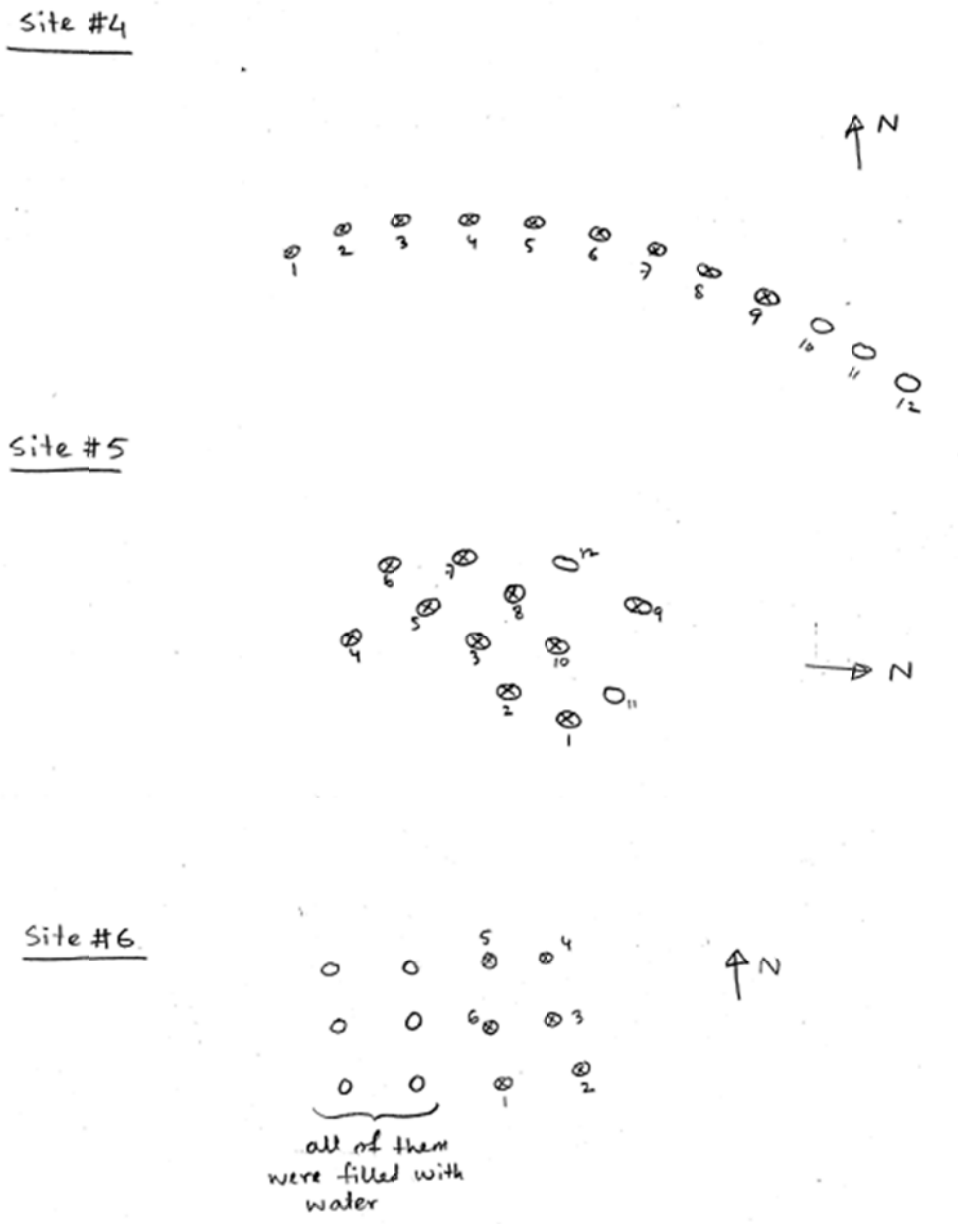

Figure 8.2 Map of site #4, #5 and #6.

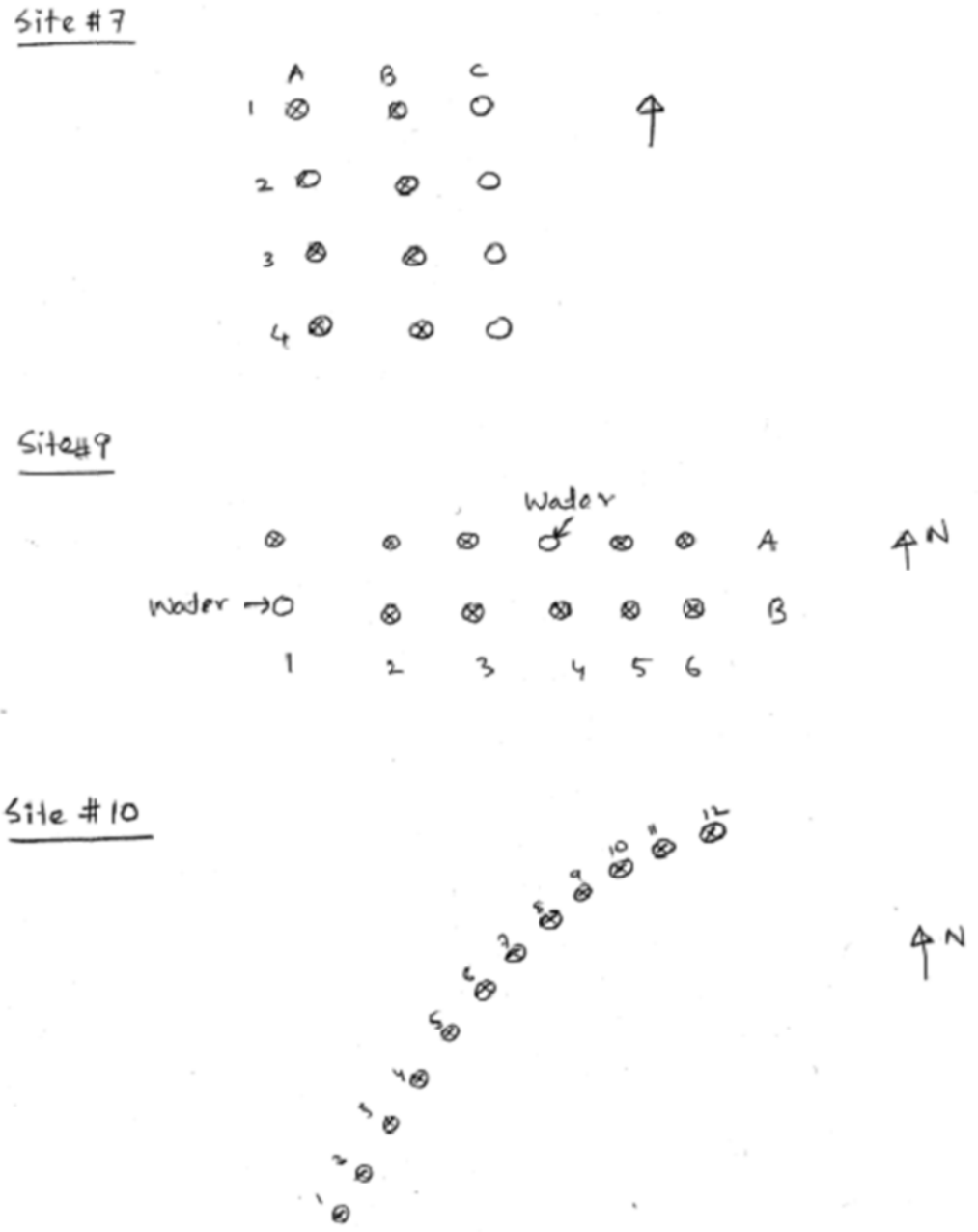

Figure 8.3 Map of site #7, #9 and #10

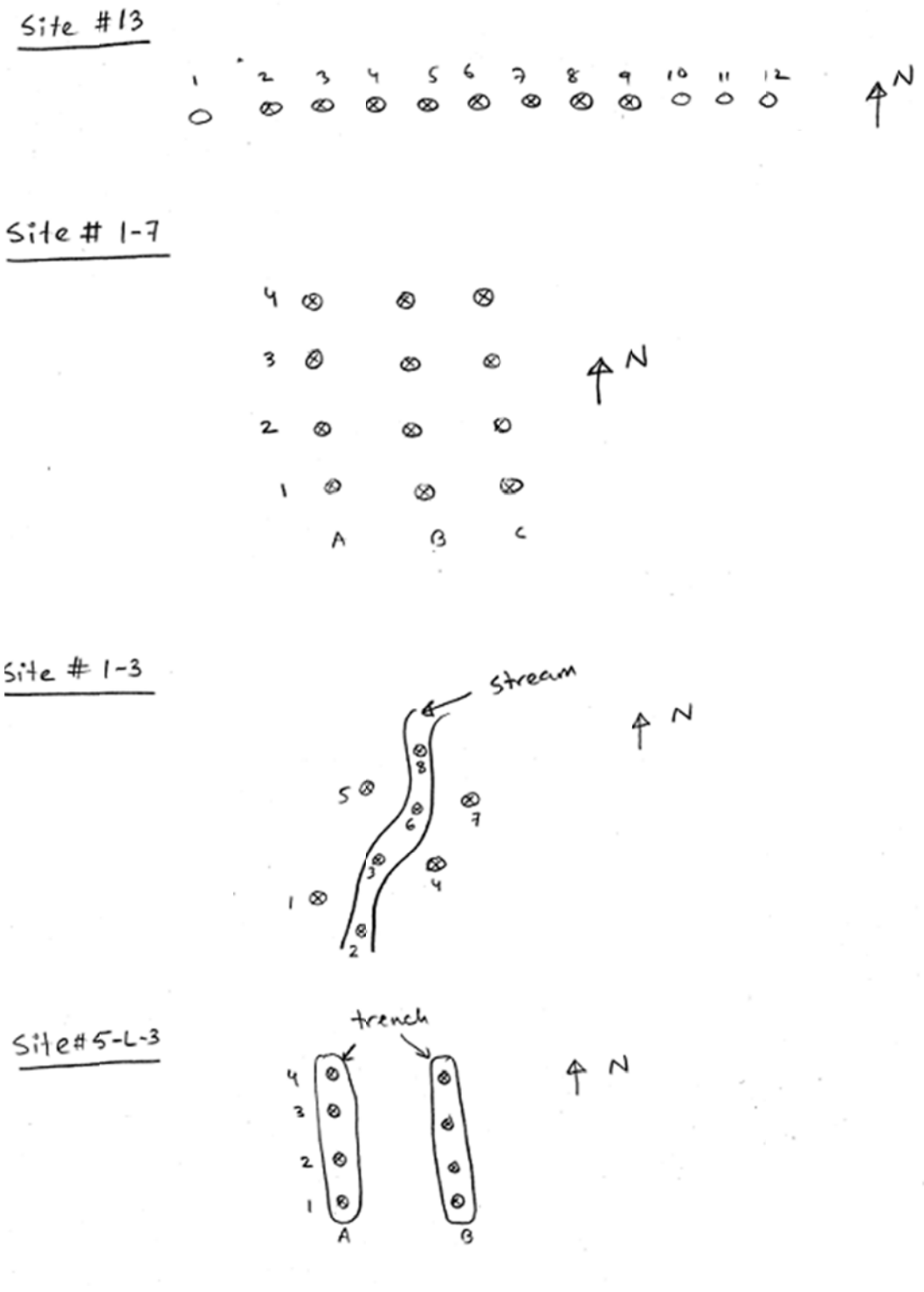

Figure 8.4 Map of site #13, 1-3, 1-7 and 5-L-3

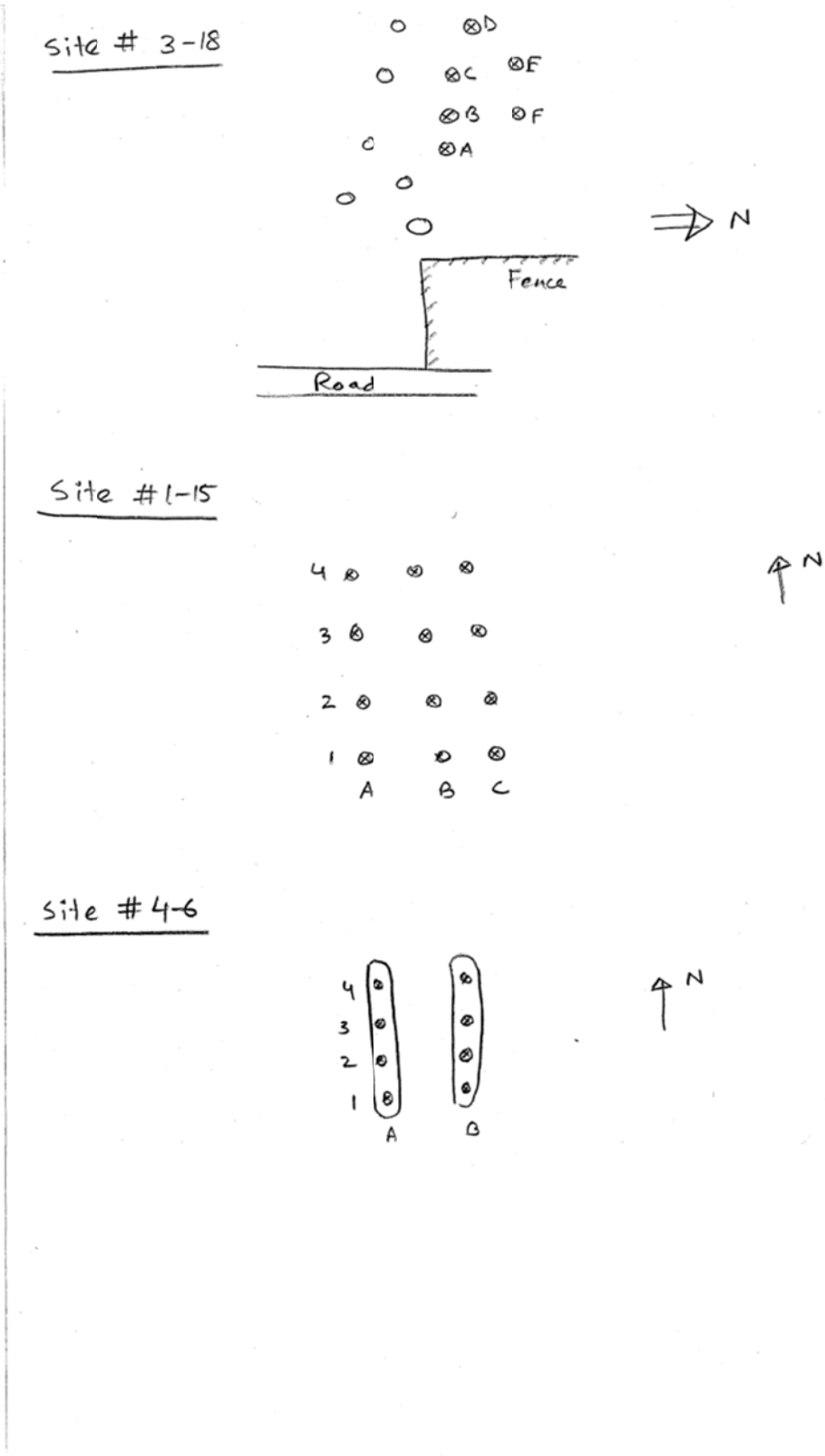

Figure 8.5 Map of site 3-18, 1-15 and 4-6.

9 Appendix C Soil distribution model

The distribution of soil types in the area are shown in Figure 9.1.The soil distribution was modeled based on 5 different sets of soil borings, including a total of 73 measurements.

These measurements were named in the following way.

Series 1:	point 1-1 to 1-15	(Braun Intertec. Engineering, Inc, 1993)
Series 2:	point 2-1 to 2-9	(American Engineering Testing Inc, 2005)
Series 3:	point 3-1 to 3-20	(American Engineering Testing Inc, 2002)
Series 4:	point 4-1 to 4-8	(Braun Intertec. Corporation, 2006)
Series 5:	point 5-1 to 5-15	(Braun Intertec Corporation, 2000)
Series 5-L:	point 5-L-1 to 5-L-5	(Braun Intertec Corporation, 2000)

For each point, the soil classification and elevation for each layer were written into an Excel-spreadsheet. The x- and y- coordinates for the borings were obtained from a digital map provided by the client, showing all the boring locations.

Using Matlab R2010a from The Mathworks, Inc., an application was developed to read all this data and present it in a 3-dimentional model. By applying different colors to each soil classification, the distribution of soil types in the area was plotted. For visualization, a reference layer was interpolated based on the elevation of the bottom of each boring. As the boring depth varied, this layer is not a true representation of the surface elevation. It still gives a decent picture of the topography in the area. The vertical scale of the plots was magnified by a factor of 10 to get a better impression of the distribution.

In addition to defining the soil classification, the boring reports also defined the geology of the soil into grades of alluvium, till or topsoil. This information was extracted from the borings as well, and presented in Figure 9.2.

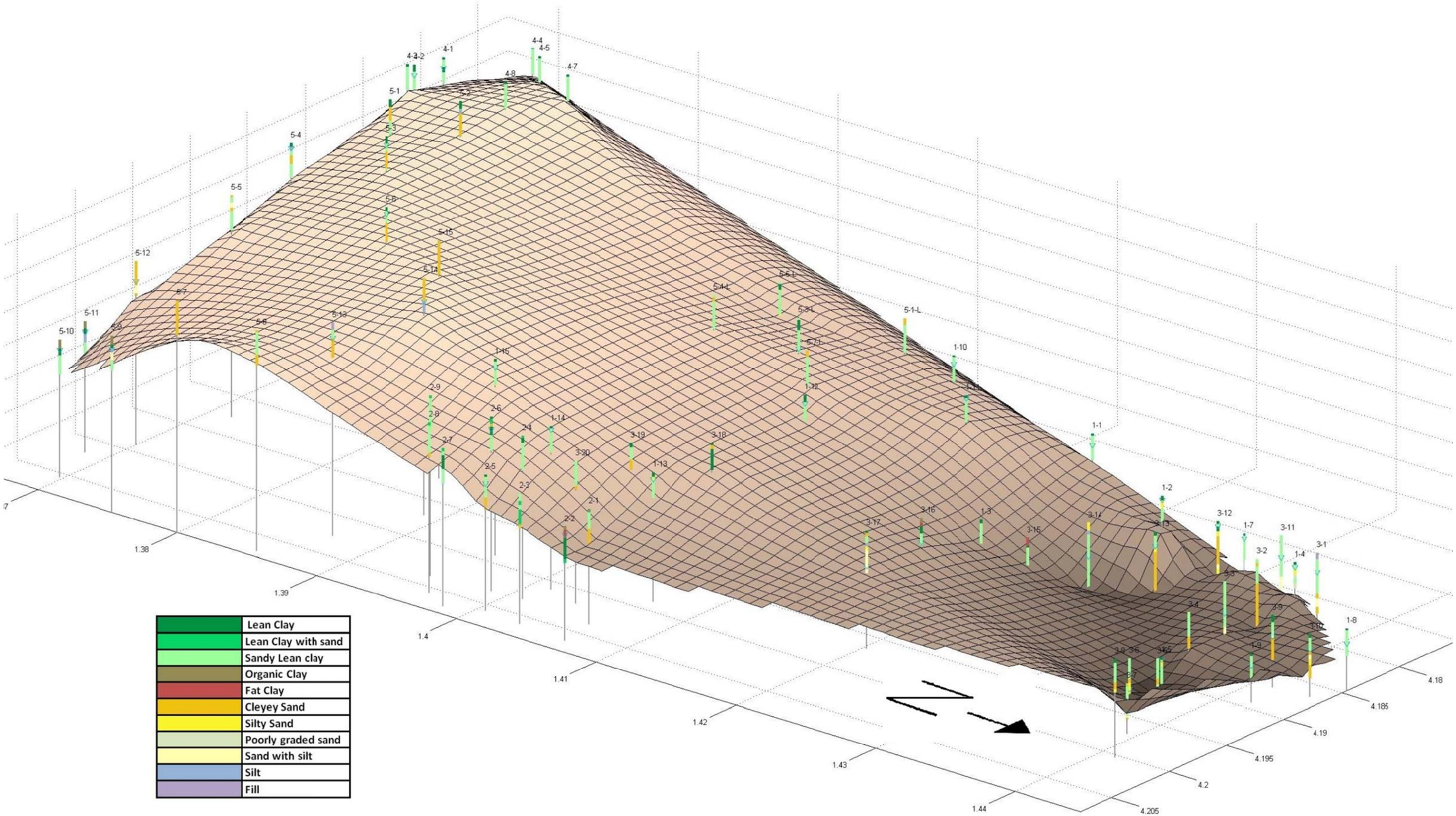

Figure 9.1 3D-model of the distribution of soil types

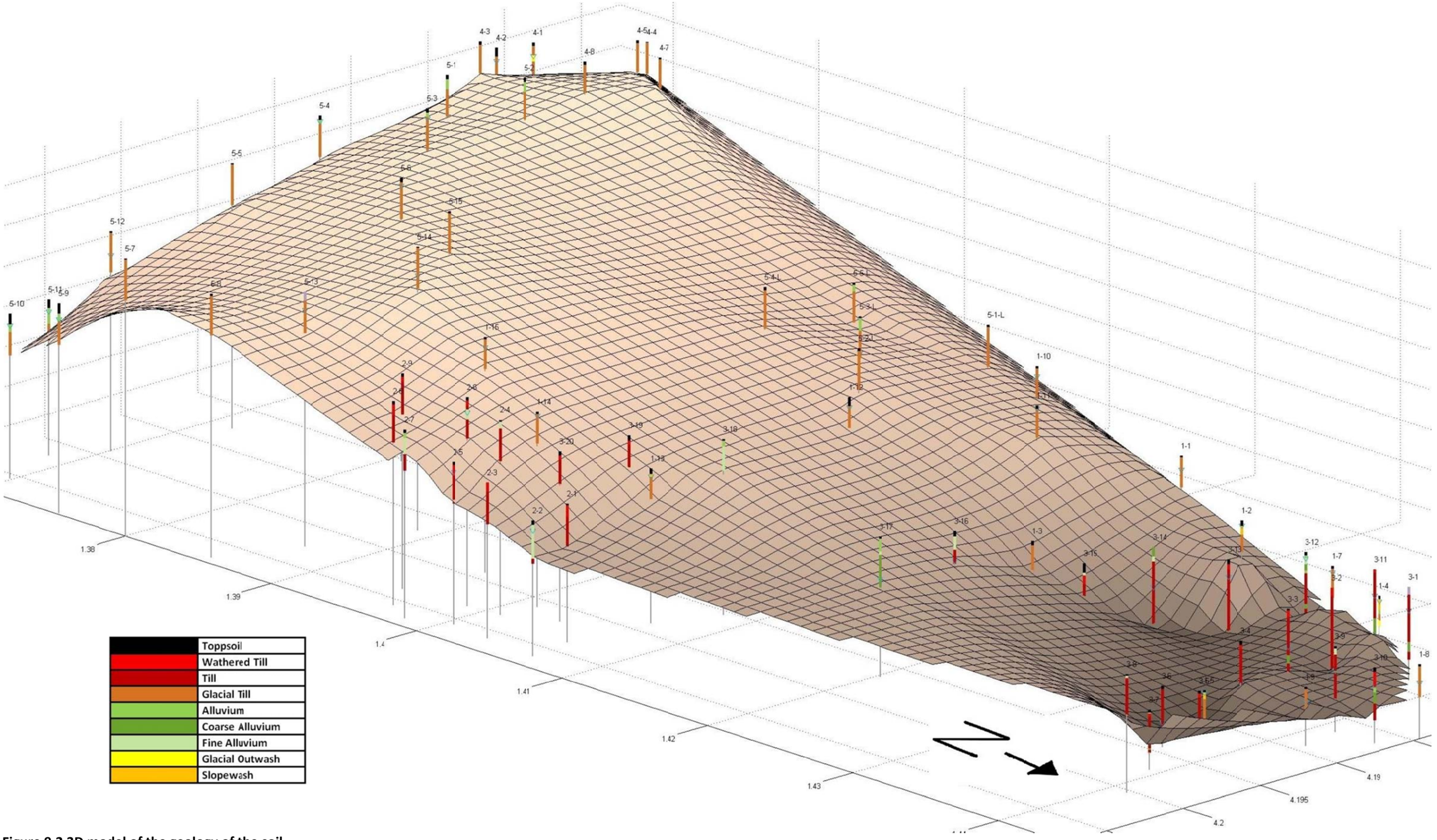

Figure 9.2 3D model of the geology of the soil

10 Appendix D Theoretical background

Measuring and estimating infiltration rate with the Excel spreadsheet

The spreadsheet minimizes the root mean square (rms) of the difference between observed time increment (Δt) and predicted time increment as well as observed head increment (ΔH) and predicted head increment, by adjusting the saturated hydraulic conductivity (K) and soil suction (C). The equation of predicted time increment and predicted head increment is obtained by equalizing two equations of potential pressure drop between the spherical source and the wetting front. Solver has been used to find the best fitting values of K and C for which the rms error of Δt or ΔH will be minimum. Prior to the wetted front reaching a minimal radius ($\sqrt{r_1^2 + L_{\max}^2}$, where r_1= radius of the MPD, L_{max}= depth of insertion into the soil), the head versus time data are neglected from the analysis because the geometry of the wetting front changes, requiring a different series of equations. Two sets of K and C are obtained, one by optimizing the Δt and the other by optimizing ΔH. Using each set of final K and C values the spreadsheet determines the predicted time for the corresponding water level and it plots both the predicted and original head vs time curve. The K and C values for which the rms regression error is lower or for which the predicted data fits better with the original data will be selected.